Optik - International Journal for Light and Electron Optics 247 (2021) 167873

Contents lists available at ScienceDirect

Optik

journal homepage: www.elsevier.com/locate/ijleo

Astigmatism in the basic Offner spectrometer

Héctor González-Núñez, Carlos Montero-Orille, Raúl de la Fuente *

Departamento de Física Aplicada, Facultade de Óptica e Optometría, Universidade de Santiago de Compostela, 15782 Galicia, Spain

ARTICLE INFO

Keywords:
Offner spectrometer
Rowland configuration
Concentric systems
Astigmatism
Optical system design

ABSTRACT

The in-plane configuration of the basic Offner spectrometer is revised. The locations of meridional and sagittal images of the slit center are analyzed when the slit is displaced in the axial direction from the usual configuration, whereas its center is kept on the Rowland circle of the concave mirror. This translates the position of the sagittal image plane and allows for the cancellation of astigmatism and meridional coma for two wavelengths while these aberrations are kept small over the whole spectral range. This is accomplished without splitting the concave mirror into two different mirrors, simplifying the design and its practical implementation. A design example is presented with excellent optical performance.

1. Introduction

Almost fifty years ago, H. Offner proposed a two mirror concentric imaging system with unit magnification which cancels all Seidel aberrations in a particular annular field: the Offner relay or Offner imaging system [1]. Later, this device was converted to an imaging spectrometer by performing two modifications. First, the convex mirror was replaced by a convex grating to provide the required light dispersion [2] and, second, as a consequence of symmetry breaking, the concave mirror was split into two mirrors to reduce second order astigmatism [3]. Really, this spectrometer provides zero astigmatism for a particular wavelength and for a particular object point, where the center of the spectrometer slit is usually placed. In the first configurations of the Offner spectrometer, the so call in-plane devices, this point was located at the plane of symmetry of the system. They were analyzed using different theoretical models [4–7]. However, new configurations were envisaged soon with the slit out of this plane: the off-plane Offner configurations [8–12]. They have the advantage that it is not necessary to split the concave mirror, but they present a good optical quality only for rather short slits. On the other hand, different variants of the Offner imaging spectrometer were analyzed to improve its imaging quality. For example, departure from concentricity [13], using non classical gratings with modified groove patterns [14], adding new refracting optical elements [15,16] or using free-form optics [17–19]. Other recent studies of the Offner imaging spectrometer can be found in references [20–25], and an excellent review of imaging spectrometers for remote sensing including the Offner design is found in [26].

In this paper, we return to the basic Offner dispersive system, that is, one concave mirror and a convex classical grating, in the in-plane configuration. We show that it is possible to reduce astigmatism in the entire spectral range, and canceling it for two different wavelengths. The key is to move the slit center from the more common configuration in which it is placed in a plane orthogonal to the optical axis containing the curvature center. This was yet considered in one of our previous works [27] but in that work we dealt with a three-component system, and we only contemplated stationary anastigmatic images at one wavelength.

* Corresponding author.
E-mail address: raul.delafuente@usc.es (R. de la Fuente).

https://doi.org/10.1016/j.ijleo.2021.167873
Received 10 February 2021; Received in revised form 2 July 2021; Accepted 21 August 2021
Available online 28 August 2021

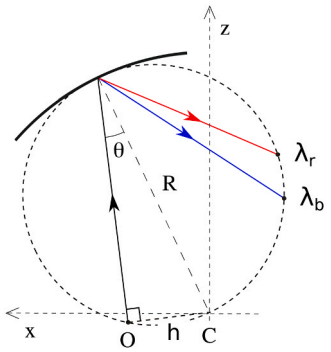

Fig. 1. Rowland circle in a spherical concave diffraction grating.

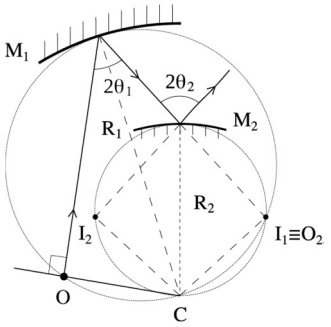

Fig. 2. Example of disposition of Rowland circles in a concentric system composed by two elements.

2. The Rowland circle

Since the Rowland circle [28] is crucial for understanding the principles of design presented here, it will be instructive to revise this concept. The Rowland circle was first defined in relation to the theory of aberrations of concave spherical diffraction gratings, but it can be applied as well to any kind of reflective or refractive spherical surface, concave or convex (in this last case, object and images are virtual). The Rowland circle is defined as the circle tangent to a spherical surface at the point of incidence of the principal ray and having its diameter equal to the radius of the surface (see Fig. 1). It has this main property [29]: when an object point belongs to this circle, it(s) meridional image(s) is (are) coma-free and belong(s) to this circle too. From the properties of circles it follows that if h is the radial coordinate of an object or image point on the Rowland circle measured from the center of curvature of the spherical surface (the so called off-center distance), it fulfills:

$$h = R \sin \theta \tag{1}$$

where R is the curvature radius and θ the angle of incidence, reflection, or refraction, as appropriate. On the other hand, the sagittal image is out of this circle, so images in the Rowland configurations present a great amount of astigmatism. This is of no concern in non-imaging spectrometers, especially in the UV range, which can be designed with only a concave diffraction grating and having the center of the slit on the Rowland circle.

However, in imaging spectrometry, astigmatism must be minimized and some elements have to be added to compensate for the astigmatism on the Rowland circle. In this case, you can take advantage of another property of the Rowland circle related to concentric systems. If an optical system is composed only by spherical elements having a common center of curvature, the complete system owns the same properties of each single surface in the Rowland disposition; that means, if the object belongs to the Rowland circle of the first optical element, the meridional image falls on the Rowland circle of the last optical element. This follows because an image on the Rowland circle of a given element also belongs to the Rowland circle of the next element, as it is shown in Fig. 2. Although it has not been demonstrated in general, the coma free property of the meridional Rowland image has been shown in some cases, namely, in the Offner and Dyson spectrometers [28,30]. In these systems, choosing wisely the radius of each surface, the position of the sagittal image can be made coincident with the meridional one, at least for a given object point of the slit and a given wavelength.

The possibility of getting anastigmatic and meridional coma-free imaging in spectrometers disposed in a concentric layout has attracted much attention. Furthermore, concentric spectrometers have been shown to present very low spatial and spectral distortion, so they have been the preferred optical configuration in many spectroscopic imaging applications.

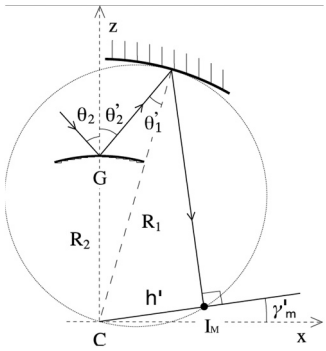

Fig. 3. Meridional image point in the Rowland circle of the concave mirror after the last reflection.

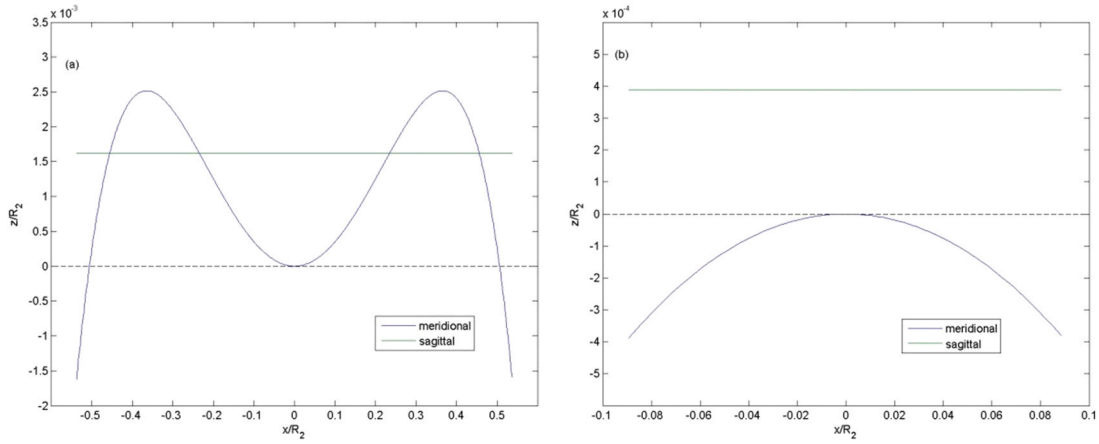

Fig. 4. (a) Locus of meridional and sagittal images for R_1/R_2=1.93. The object is located at the beginning of the meridional curve. (b) Same as 4a but R_1/R_2=2.03. These curves are representative of the general cases $R_1/R_2 < 2$ and $R_1/R_2 \geq 2$.

3. Locus of meridional and sagittal images

In this section, a basic Offner spectrometer with an object point located on the Rowland circle of the concave mirror is considered. We will concentrate our attention in the image plane, after reflection at the grating. In the light of the above discussion, the spectral meridional images belong to the corresponding Rowland circles of the concave mirror after the second reflection. The x, z coordinates of these images (x'_m, z'_m) can be related to the angle of diffraction of the corresponding principal ray, θ'_2. According to the geometry of Fig. 3:

$$\begin{aligned} x'_m &= -R_2 \sin\theta'_2 \cos\gamma'_m \\ z'_m &= -R_2 \sin\theta'_2 \sin\gamma'_m \end{aligned} \tag{2}$$

where γ'_m is the polar angle of the meridional image point. and the invariance of the off-center distance by reflection (or refraction) in a concentric system has been applied:

$$h' = -R_1 \sin\theta'_1 = -R_2 \sin\theta'_2 \tag{3}$$

The negative signs in the above expressions are due to our sign convention: positive angles have been taken for counterclockwise rotation about an axis or about a normal to a surface, while the radii R_1 and R_2 were taken positive. On the other hand, note that the angles are related by the following equation: $\gamma'_m = \theta'_2 - 2\theta'_1$.

In Fig. 4 the locus of meridional image points corresponding to different diffraction angles, that is, different wavelengths, are represented for some particular radii ratios R_1/R_2. Note that these curves also represent the possible locations of the object point whenever it belongs to the Rowland circle of the first mirror (in this case, by convention, only the left part of the curve, $x'_m<0$, must be considered). In Fig. 4(a) the radius ratio is less than two. In this case, the main characteristics of these curves are the following:

i) They are symmetric with respect to the z axis.

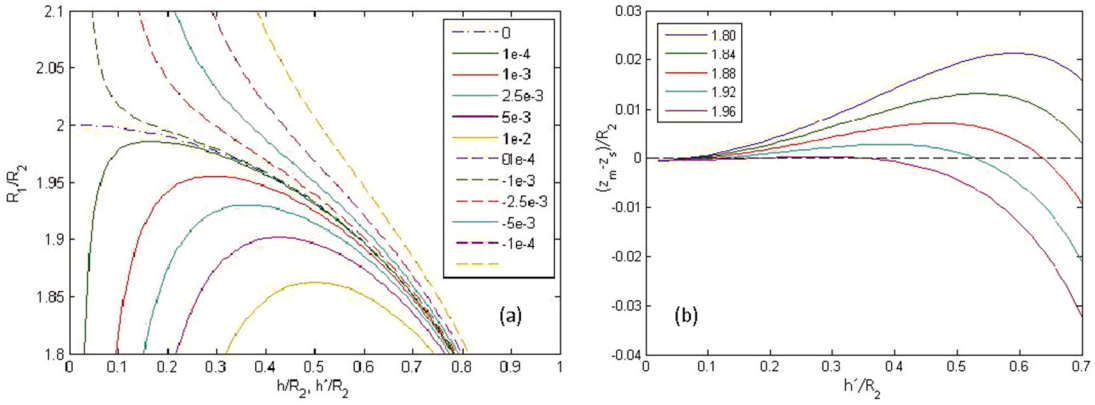

Fig. 5. (a) Map of Rowland points. Curves are labeled by the value of the z-coordinate of the object normalized to R_2. (b) normalized second order astigmatism versus normalized image off-center distance for different radius ratio R_1/R_2.

ii) They cross the x-axis at$\theta'_1 = \theta'_2/2 = \pm\arccos(0.5R_1/R_2)$, being positive between these two values (except for $\theta'_1 = \theta'_2 = 0$where their value is zero).

iii) At their maximums they fulfill:

$$\tan\gamma'_m = 2\tan\theta'_1 - \tan\theta'_2 \tag{4}$$

iv) The position of the specular meridional image (zero diffraction order) is obtained from the position of the object by specular reflection with respect to the z-axis. That means x'_m=-x, z'_m=z, h'=h and $\theta'_2 = -\theta_2$, where x, z, h are the x, z-coordinates and off-center distance of the object point, respectively, and θ_2 is the angle of incidence of the principal ray on the grating.

v) Meridional images for positive diffraction order are on the left of the specular image.

The shapes of the curves are very different for $R_1/R_2 \geq 2$ (see Fig. 4b). In that case the curves are tangent to the x-axis at $\theta'_1 = \theta'_2 = 0$ and decrease symmetrically as the angle increases.

Note that the normalized position of Rowland images only depends on the radius ratio (the radius R_2 acts as a scale). It does not depend on the object position, whenever it is in the Rowland circle at the first reflection in the concave mirror. The object position only fixes the position of the meridional specular image (the image for zero wavelength). On the other hand, the relation between image position and wavelength λ is dictated by the grating equation:

$$\sin\theta_2 + \sin\theta'_2 = mg\lambda \tag{5}$$

where g is the grating groove density and m the diffraction order. Depending on the value of g and the object position (which defines angle of incidence at the grating, θ_2), the image for a given wavelength is placed in a particular point of the meridional image curve in Fig. 4.

With respect to the positions of sagittal images they are bound by the following invariant [16]:

$$\sin\theta_2\tan\gamma = -\sin\theta'_2\tan\gamma'_s \tag{6}$$

which relates the z-coordinates of sagittal images, z_s', and object point, z, as follows:

$$z'_s = -R_2\sin\theta'_2\frac{\sin\gamma'_s}{\cos(\gamma'_s-\gamma'_m)} = -z\frac{\cos(\gamma'_s)}{\cos(\gamma'_s-\gamma'_m)\cos(\gamma)} \tag{7}$$

For typical configurations, the radius ratio is close to two and the object is very closed to the x-axis, so the polar angles γ and γ'_m are very closed to zero. Therefore, $z'_s \approx -z$, and the position of sagittal images is constant (see Fig. 4).

4. Anastigmatism

In this section we analyze anastigmatic imaging in the basic Offner spectrometer with an object point in the Rowland circle of the concave mirror at the first reflection. The condition of anastimatism is:

$$z'_m = z'_s = -z \tag{8}$$

For configurations where $R_1/R_2 \geq 2$ we have the behavior shown in Fig. 4b: all images are astigmatic. However, when $R_1/R_2 < 2$, there are several anastigmatic images depending on the object position. If the object is at $z>0$, the sagittal line is at $z<0$ and there are

Table 1
Design parameters.

Slit length (mm)	9.5
Spectral band (nm)	900–1700
f-number	2.75
Diffraction order	+1
Grating density (gr/mm)	175
Grating radius (mm)	50
Radius ratio	1.885
Coordinates of slit center (x_0,z_0) (mm)	(−33.98, −0.33)

two anastigmatic images (remember that we consider the object at $x<0$): one on its left and the other on its right. Therefore, they correspond to diffraction orders of different sign. Otherwise, if $z<0$, there are up to four anastigmatic images (see Fig. 4a). However, the spectra cannot expand to cover all these images because the diffraction grating generates vignetting. Thus, we are left to consider only two anastigmatic images, either to the left or to the right of the z-axis. In the particular case in which the sagittal line touches the meridional curve at its maximum the image is anastigmatic and stationary, that is, the derivative of astigmatism with respect to wavelength also vanishes. If the object is moved away from the z axis, further anastigmatic images will not be found. Note that for the typical configuration in which the object is located on the x-axis, there are three anastigmatic images. However, one of them overlaps the object, other is its specular image and the last one is on the optical axis.

We can get a more general vision looking at Fig. 5(a) where it is plotted a map of points in the Rowland circle as a function of radius ratio and off-center distance. Each curve corresponds to a given value of the z-coordinate of the object. The continuous curves are for $z>0$ and the dashes curves for $z<0$. The dotted-dashed line corresponds to $z=0$. Considering that the object is on a curve with $z=z_0$, and according to Eq. (8), anastigmatic images fit in the curve $z=-z_0$. Drawing a horizontal line at a given radius ratio, the intersection of this line with those curves provides the off-center distance for the object and its anastigmatic images corresponding to this radius ratio.

As it was mentioned above, there are not anastigmatic images for objects in the Rowland circle if $R_1/R_2 \geq 2$, since in this case there are only curves with negative z. If the object is located at a point with $z>0$, there are two possible positions in the Rowland circle, being, in principle, the position closer to the curvature center of the surfaces preferable since it corresponds to a more paraxial regime. In this case, the image curve contains a single anastigmatic image at each side of the z axis. The spectra can be expanded towards the curvature center which corresponds also to a more paraxial region. On the other hand, placing the object at a point with $z<0$, allows for the use of the +1 diffraction order, enabling the reduction of the astigmatism over the whole spectral range by using the two corresponding anastigmatic images. Besides, you must be careful to locate the spectra near the stationary anastigmatic point to limit the amount of anastigmatism over the whole spectra. This is an advantage over a configuration in which the object has positive z-coordinate. Indeed, in Fig. 5(b), the astigmatism, calculated in a good approximation as z'_m-z'_s, is plotted as a function of h′ for several radius ratios R_1/R_2. It is clear from this figure that for a given spectral range (Δλ or Δh') there is an optimum radius ratio which minimizes the astigmatism over the whole spectral range. This will be considered in the next section.

5. Simulations

Some simulations using Matlab [31] and Oslo design software [32] were performed to show that basic Offner spectrometers of high optical quality can be designed provided that second order astigmatism for the images of the slit center is reduced. We devised a design procedure in Matlab which comprises the following steps:

i) the specifications of the spectrometer to be designed are considered, namely, the spectral band (λ_-, λ_+), the lengths of both slit and spectral image, the diffraction order and the f-number (f/#).
ii) An initial value of the grating density g is assumed.
iii) The curvature radius of the grating is calculated by [16]:

$$R_2 = \frac{h_{spec}}{|m|g\Delta\lambda} = 50\text{mm} \tag{9}$$

where h_{spec} is the length of the spectral image, for the considered spectral band, $\Delta\lambda = \lambda_+ - \lambda_-$.
iv) Vignetting is avoided, approximately, by imposing the following condition: $\sin\theta'_{2v} = \mp 1/(f/\#)$ where $\theta'_{2v}$is the angle of diffraction of the principal ray for the wavelength, λ_v, which is diffracted closest to the diffraction grating, and the minus sign applies if light is diffracted to the left side of the z-axis.
v) The grating equation is used to calculate the angle of incidence at the grating at λ_v: $\sin\theta_{2v} = mg\lambda_v \pm 1/(f/\#)$,
vi) A value of the radius ratio$R_1/R_2$is established. Eqs. (2) and (3) are applied in the object domain (angles without single quotation mark) to calculate de coordinates of the object. Then, these equations are used to calculate the z-coordinate of the meridional image for every wavelength in order to compute the second order longitudinal astigmatism as $z_m - z_s \cong z_m + z$.
vii) Step vi) is performed iteratively for a set of radius ratios and the astigmatism is minimized in the full spectral range by minimizing the following sum, from λ_- to λ_+: $\sum(z_m - z_s)^2$. This gives an optimum radius ratio.
viii) The steps ii) to vii) are iterated until $z_m - z_s|_{\lambda_-} = z_m - z_s|_{\lambda+}$, that is, g is chosen so that the second order astigmatism is minimized at the edges of the spectral band.

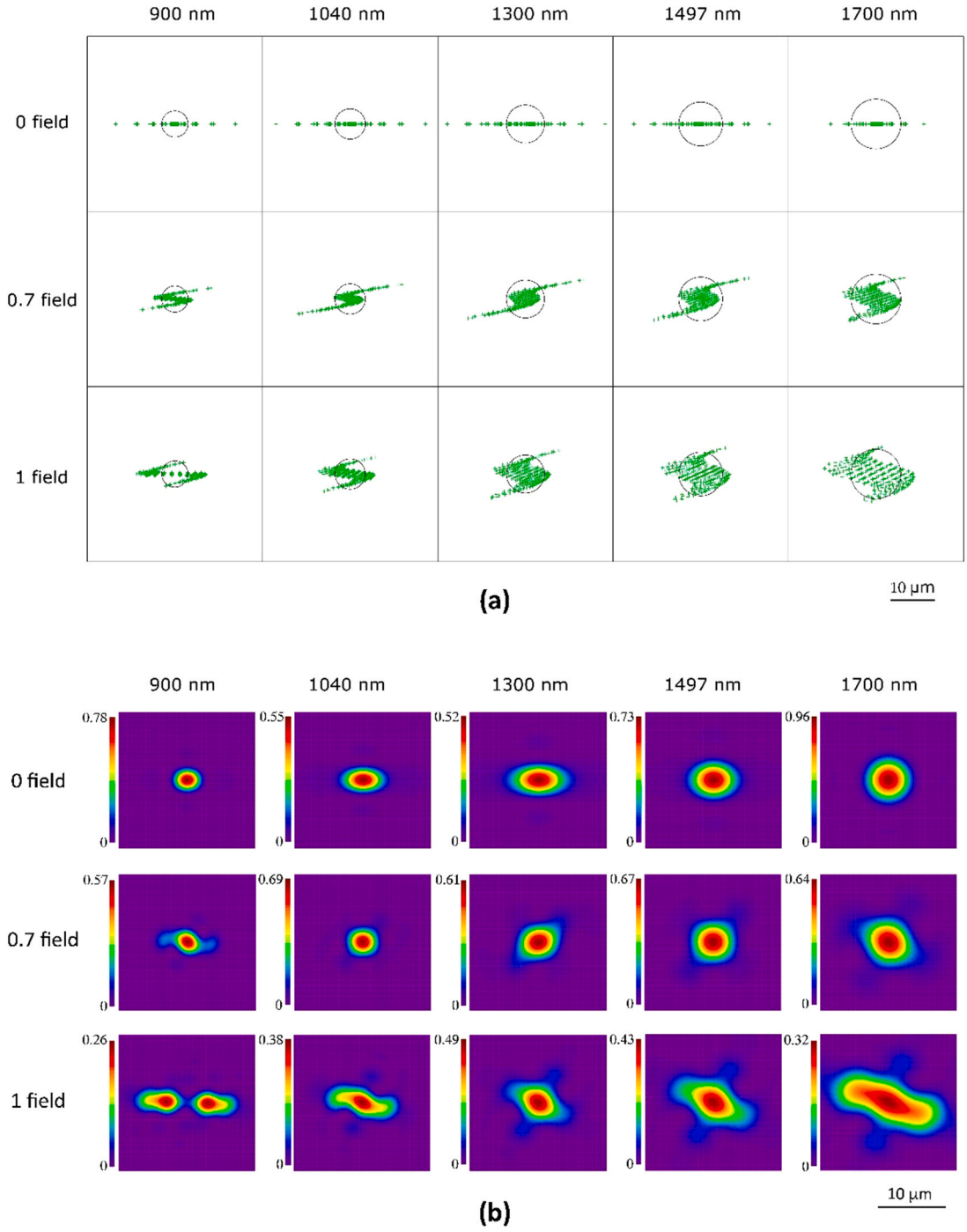

Fig. 6. (a) Spot diagrams for 0, 0.7 and full field, and selected wavelengths the Airy disk is also plotted. (b) The PSF for the same fields and wavelengths. Numbers in the upper left corner of each plot correspond to the Strehl ratio. Each plot is enclosed in a square of 20 μm of side.

After completing these steps, there may still be some vignetting (this can be checked with the Oslo design software), so we can start the design procedure from a slightly smaller f-number and finally set the f-number to the one given in the specifications.

In order to check this design procedure, we designed an Offner spectrometer in the SWIR (900–1700 nm), the sensitive spectral range of a common InGaAs sensor. We considered a typical sensor size 9.6×7.68 mm^2 with 15 μm square pixels and a f-number, f/#=2.75. The sensor is located at the sagittal image plane: the spectrum, with spatial extension h_{spec}=7 mm, lies along the shorter sensor dimension; and we choose a slit length of 9.5 mm. Then, the design procedure described above was applied. The spectrometer specifications are shown in rows 1–4 in Table 1 while rows 5–8 display the results of the design. All of these parameters are calculated

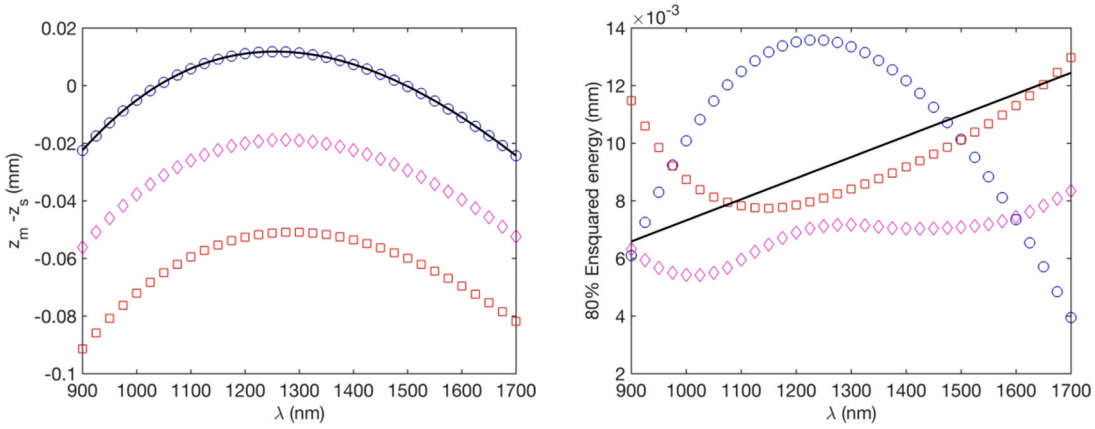

Fig. 7. (a) Second order astigmatism calculated with Oslo Software for 0 (blue points), 0.7 (purple points) and full field (red points). (b) 80% ensquared energy versus wavelength for 0, 0.7 and full field. The black curve in (a) correspond to the result obtained through the design procedure implemented in Matlab and the black line in (b) correspond to the diffraction limit. (For interpretation of the references to color in this figure legend, the reader is referred to the web version of this article.).

considering $\lambda_v=\lambda_+=1700$ nm, the wavelength that diffracts closest to the grating. Finally, the whole spectrometer has a size of $35\times100\times95$ mm.

In Fig. 6(a) we represent different spot diagrams calculated with Oslo design software after data entry from Table 1, for 0, 0.7 and full field (4.75 mm) at selected wavelengths. These are the center and extreme wavelengths, the anastigmatic wavelengths (1040 and 1497 nm). It is seen that at 0 field, astigmatism is the relevant aberration for all the spectral images and the degree of astigmatism is similar in all the cases. This means that higher order astigmatisms are significant, once second order astigmatism has been minimized. At 0.7 and full field, every spot diagram has an S shape, greater for larger fields and more elongated for smaller wavelengths. In Fig. 6 (b) the corresponding point spread functions (PSF) are represented. Because of the effect of diffraction, the spatial resolution (vertical dimension) decreases with respect to the values expected from the spot diagrams, being the PSF shape elliptical at 0 field points. Note that except the last one, all PSFs are contained in the 15-micron camera pixels. This corresponds to a spectral resolution (horizontal dimension) lower than 0.9 nm. As it is typical in the in-plane Offner configuration, spatial resolution is better than spectral resolution. Note also that the Strehl ratios at 0 and 0.7 fields achieve outstanding values.

In Fig. 7a we represent the spectral curves of second order longitudinal astigmatism calculated for the slit center by Oslo and Matlab software from the data of the design made by the latter. We also represent the corresponding astigmatism curves for the images of the 0.7 and full field points on the slit. It is seen that for any point on the slit and wavelength the longitudinal second order astigmatism is less than 0.09 mm. Furthermore, the curves are very similar except for a vertical translation. In Fig. 7b we represent the spectral curves of 80% ensquared energy for the same slit points. All the curves are contained in a square of side less than 14 μm, which is smaller than the size of a pixel sensor. These curves include the contribution of astigmatism and higher order aberrations. As commented in Ref. [4], main contributions come from third order sagittal coma and fourth order spherical aberration. It is seen that for the two boundaries of the spectrum, aberrations increase as we move away the slit center. However, for the center of the spectrum, aberrations are greater for the slit center, and they are the greatest ones. This is consistent with the great length of the astigmatic lines shown in Fig. 6. It is worth noting that the data in Table 1 corresponds to the final design, without any further optimization. However, we also checked if an optimization would improve noticeably this final design. So, by using the Oslo design software and its optimization routines, we allowed the decentering of the elements in the XZ plane, the tilting of the image plane around the y-axis, and the curvature of the first mirror, to vary freely. The result was an optimized system out of concentricity whose worst image point had an RMS spot radius of 5.2 μm; a value only a little better than the one (5.6 μm) of our final design. This is a very small improvement that does not compensate for the inconveniences of taking the system out of concentricity; something especially relevant during alignment tasks in an experimental setup.

On the other hand, we also compared our design with the classical Offner imaging spectrometer, that is, the configuration where both slit and image plane are in a plane perpendicular to the z-axis which contains the center of curvature of the system. Since in this configuration and are zero the following relationship is fulfilled: $R_1=2R_2\cos\theta_1$, being θ_1 the minimum angle which avoids vignetting. By considering these constrains we calculated a new radius ratio of 1.859 and new coordinates of the slit center $x_0=-34.25$ mm and $z_0=0$ mm. Once introduced these values in the Oslo software, we obtained an RMS spot radius of 40.39 μm for the best image point of this classical system, and the Strehl ratios reach very low values (less than 0.07). That corresponds to a very low-quality design. Of course, very good designs can be achieved breaking the layout symmetry by splitting the concave mirror into two mirrors of different radii, but this would be contrary to the purpose of the present work: to obtain an Offner design of excellent quality with a very simple configuration of only a concave mirror and a convex diffraction grating.

6. Conclusions

The locus of meridional and sagittal images of a point object in a basic Offner spectrometer has been analyzed. The meridional curve is symmetric with respect to the z axis and has a zero value at the center of curvature of the system and, for $R_1/R_2 < 2$, two other symmetric points. Furthermore, the curve is bounded at z>0. On the other hand, the sagittal curve is, for all the purposes, a line perpendicular to the z axis. This allows for changing the astigmatism by only translating the position of the object along the z-axis and placing the imaging sensor in the sagittal image plane. This is true for small z-coordinates of the object, which is the case in most practical spectrometers. Anastigmatic images at up to four wavelengths are found if the radius ratio R_1/R_2 is less than two. However, only two images are available provided that vignetting is avoided at the central part of the spectrum. A simple design has been presented showing the quality of this basic Offner spectrometer.

Funding

Xunta de Galicia, Consellería de Educación, Universidades e FP, Spain, Grant GRC number ED431C2018/11 and ED431E2018/08.

Declaration of Competing Interest

The authors declare that they have no known competing financial interests or personal relationships that could have appeared to influence the work reported in this paper.

References

[1] A. Offner, Unit Power Imaging Catoptric Anastigmat, U.S. Patent US3748015A.
[2] L. Mertz, Concentric spectrographs, Appl. Opt. 16 (1977) 3122–3124.
[3] M.P. Chrisp, Convex Diffraction Grating Imaging Spectrometer, U.S. Patent US5880834A (1999).
[4] H.éctor González-Núñez, Xesús Prieto-Blanco, Raúl de la Fuente, Pupil aberrations in Offner spectrometers, J. Opt. Soc. Am. A 29 (2012) 442–449.
[5] Yiqun Ji, Rudong Xue, Weimin Shen, New design method based on sagittal flat-field equipment of Offner type imaging spectrometer, Proc. SPIE 8200 (2011) 82000D.
[6] Meihong Zhao, Yanxiu Jiang, Shuo Yang, Wenhao Li, Geometric aberration theory of Offner imaging spectrometers, Sensors 19 (2019) 4046.
[7] Jialun Zhang, Yuquan Zheng, Chao Lin, Zhenhua Ji, Hao Wu, Analysis method of the Offner hyperspectral imaging spectrometer based on vector aberration theory, Appl. Opt. 60 (2021) 264–275.
[8] R.L. Lucke, Out-of-plane dispersion in an Offner spectrometer, Opt. Eng. 46 (2007), 073004.
[9] X. Prieto-Blanco, C. Montero-Orille, H. González-Nuñez, M.D. Mouriz, E. López Lago, R. de la Fuente, The Offner imaging spectrometer in quadrature, Opt. Express 18 (2010) 12756–12769.
[10] X. Prieto-Blanco, H. González-Nuñez, R. de la Fuente, Off-plane anastigmatic imaging in Offner spectrometers, J. Opt. Soc. Am. A 28 (2011) 2332–2339.
[11] Qiao Pan, Xinhua Chen, Jiankang Zhou, Quan Liu, Zhicheng Zhao, Weimin Shen, Manufacture of the compact conical diffraction Offner hyperspectral imaging spectrometer, Appl. Opt. 58 (2019) 7298–7304.
[12] Qiao Pan, Xinhua Chen, Jiankang Zhou, Zhicheng Zhao, Weimin Shen, Design and measurement of convex grating in conical diffraction Offner spectrometer, Opt. Eng. 58 (2019) 1.
[13] S.H. Kim, H.J. Kong, J.U. Lee, J.H. Lee, J.H. Lee, Design and construction of an Offner spectrometer based on geometrical analysis of ring fields, Rev. Sci. Instrum. 85 (2014), 083108.
[14] L.Q. Xiang, T. Mikes. Corrected Concentric Spectrometer Patent WO1999056096 (1999).
[15] X. Prieto-Blanco, R. de la Fuente, Compact Offner–Wynne imaging spectrometers, Opt. Commun. 328 (2014) 143–150.
[16] Jing Lin, Su Wu, Lei Yu, Broadband astigmatism-free Offner imaging spectrometer with high resolution, Appl. Opt. 59 (2020) 1110–1116.
[17] J. Reimers, A. Bauer, K.P. Thompson, J.P. Rolland, Freeform spectrometer enabling increased compactness, Light Sci. Appl. 6 (2017) 17026.
[18] Lidong Wei, Lei Feng, Jinsong Zhou, Juanjuan Jing, Yacan Li, Optical design of Offner-Chrisp imaging spectrometer with freeform surfaces, Proc. SPIE 10021 (2016).
[19] Jialun Zhang, Chao Lin, Zhenhua Ji, Hao Wu, Chengliang Li, Bowen Du, Yuquan Zheng, Design of a compact hyperspectral imaging spectrometer with a freeform surface based on anastigmatism, Appl. Opt. 59 (2020) 1715–1725.
[20] Y. Huang, Zi Pei, R. Hong, B. Li, D. Zhang, B. Xu, Z. Ni, S. Zhuang, Non-approximate method for designing Offner spectrometers, Optik 125 (2014) 4578–4582.
[21] Yiqun Ji, Jianxin Li, Jiangkang Zhou, Weimin Shen, Analytical design and implementation of an imaging spectrometer, Appl. Opt. 54 (2015) 517–526.
[22] Jiacheng Zhu, Weimin Shen, Analytical design of athermal ultra-compact concentric catadioptric imaging spectrometer, Opt. Express 27 (2019) 31094–31109.
[23] Yu-Hang Shen, Zheng-Ji Ni, Yuan-Shen Huang, Bin Sheng, Bang-Lian Xu, Mo-Qiang Guo, Meng-Jing Xu, Analytical design of a high-performing +1st order diffraction convex grating imaging spectrometer, Appl. Opt. 59 (2020) 3760–3765.
[24] M.P. Chrisp, R.B. Lockwood, M.A. Smith, G. Balonek, C. Holtsberg, K.J. Thome, K.E. Murray, P. Ghuman, Development of a compact imaging spectrometer form for the solar reflective spectral region, Appl. Opt. 59 (2020) 10007–10017.
[25] Nikolay Kazanskiy, Nikolay Ivliev, Vladimir Podlipnov, Roman Skidanov, An airborne Offner imaging hyperspectrometer with radially-fastened primary elements, Sensors 20 (2020) 3411.
[26] Pantazis Mouroulis, Robert O. Green, Review of high fidelity imaging spectrometer design for remote sensing, Opt. Eng. 57 (2018) 1.
[27] X. Prieto-Blanco, C. Montero-Orille, B. Couce, R. de la Fuente, Analytical design of an Offner imaging spectrometer, Opt. Express 14 (2006) 9156–9168.
[28] H.A. Rowland, Philos. Mag., 13, 477 (1882).
[29] H. Beutler, The theory of the concave grating, J. Opt. Soc. Am. 35 (1945) 311–350.
[30] C. Montero-Orille, X. Prieto-Blanco, H. González-Núñez, R. de la Fuente, Design of Dyson imaging spectrometers based on the Rowland circle concept, Appl. Opt. 50 (2011) 6487–6494.
[31] MATLAB, version 7.14.0.739 (R2012a). Natick, Massachusetts: The MathWorks Inc., 2010.
[32] OSLO is a registered trademark of Lambda Research Corporation, 25 Porter Road, Littleton, MA 01460.